Investigation of Dimethylammonium Solubility in MAPbBr 3 Hybrid Perovskite: Synthesis, Crystal Structure, and Optical Properties

Investigation of Dimethylammonium (DMA) Solubility in $MAPbBr_3$ Hybrid Perovskite: Synthesis, Crystal Structure and Optical Properties

*By Camilla Anelli,[a] Michele R. Chierotti,[b] Simone Bordignon,[b] Paolo Quadrelli,[a] Daniela Marongiu [c] , Giovanni Bongiovanni [c], Lorenzo Malavasi[a,]**

[a]Department of Chemistry and INSTM, Viale Taramelli 16, Pavia, 27100 (Italy); Department of Physics and CNISM, Via Bassi 6, Pavia, 27100 (Italy)

[b]Department of Chemistry and NIS Centre, V. Giuria 7, Torino, 10125 (Italy)

[c]Department of Physics, University of Cagliari, S.P. Monserrato-Sestu km 0.7, Cagliari, 09042, Italy.

Corresponding Author

*Lorenzo Malavasi, email: lorenzo.malavasi@unipv.it; tel. +39 382 987921

Abstract

The possible existence of mixed MA/DMA lead bromide hybrid perovskites of general formula $MA_{1-x}DMA_xPbBr_3$ ($0 \leq x \leq 1$) was investigated. A combined x-ray diffraction and solid-state NMR approach indicates that DMA can be incorporated up to about $x = 0.30$ while retaining the cubic lattice of $MAPbBr_3$. By increasing the DMA-content (x) the absorption shows a progressive blue shift and the band-gap moves from about 2.17 eV ($x = 0$) to about 2.23 ($x = 0.30$) with a concomitant slightly faster recombination in the mixed cation powders.

Introduction

Mixed A-site cation hybrid perovskites of general formula ABX_3 have recently attracted significant interest in the community due to very high efficiencies shown by the perovskites solar cells (PSC) which employ such semiconductor layers, exhibiting strong bandgap photoabsorption.[1-4] The interest in such a mixed system is various and aims to tune their optical properties, improving their chemical stability and exploring their basic physical properties.[5-8] The most efficient mixed hybrid perovskites present two organic cations, usually methylammonium (MA) and formamidinium (FA), together with a inorganic monovalent cation, such as Cs^+ or Rb^+, on the A-site of the perovskite structure.[9] Also the halide site is often mixed, with the iodide/bromide system being the most intensively explored.[10] The wide tunability of perovskite crystal structure allowed a very rich compositional engineering research which has been object of intense studies in the last years.[9] The main result is that the introduction of the mixing on A site cations and X site halide anions is the most promising approach to enhance the stability against phase separation/polymorphism in perovskite solar cells (PSSCs).[1] The presence of MA/FA mixed cations is nowadays recognized as a key tool to improve the stability of the PSSCs as well as to extend the absorbance towards the infrared region.[11] Other effective active layers are made of triple systems such as MA/FA/Cs, where Cs^+ cation is thought, through entropy arguments, to further stabilize the perovskite structure. Cells made of a triple cation mixed (Cs/FA/MA)Pb(I/Br) system generated a power output of 21.1%.[12] On the other hand, the possible exploration of other mixed compositions is of current interest for the reasons reported above. In particular, the formation of MA-based mixed systems with bigger cations such as dimethylammonium (DMA) and/or trimethylammonium (TMA) has not yet been explored in the literature. In particular, there is a significant interest in investigating, DMA-based mixed systems. Indeed, it was recently realized that in solution-processed methods, where dimethylformamide (DMF) is used as a solvent in presence of

halogenated acids, the dimethylammonium cation is formed, which may lead to the formation of $DMAPbI_3$ and/or be included into the perovskite structure.[13] Very recently, a first paper addressing the possible formation of mixed MA/$DMAPbI_3$ system has been published.[14] By means of solid state NMR, the authors demonstrate the possible incorporation of DMA up to about 15% into the $MAPbI_3$ structure, with a beneficial effect on the photovoltaic cells performance.[10] However, no specific structural and optical data are reported on the mixed compositions. Moreover, another recent work by Ke and co-workers pointed out that the all-inorganic $CsPbI_3$ stable perovskite, when synthesized in PSSCs with the use of HI, is, in fact, the hybrid perovskite $Cs_{1-x}DMA_xPbI_3$.[15] In this work it was reported that the solubility limit of DMA in $CsPbI_3$ reaches a value of about 0.5, and that solar cells based on the representative composition $Cs_{0.7}DMA_{0.3}PbI_3$ can achieve an average power conversion of about 10%.[15]

Coming to other halides, to the best of our knowledge, only the $DMAPbBr_3$ system has been currently synthesized and investigated, while no information are available on MA/DMA mixed lead halide compositions.[7] The study of these latter systems is also of basic interest to further test the applicability of the well-known tolerance factor (*t*) concept in the field of organic-inorganic hybrid perovskites.[16] As a matter of fact, the DMA cation has an effective radius (r_{Aeff}) of about 272 pm, while the MA cation has a r_{Aeff} of about 217 pm.[7,16]

Due to the motivations reported above, in the present paper we afforded the preparation and characterization of the $MA_{1-x}DMA_xPbBr_3$ solid solution, with the aim to define the possible existence of this mixed system (and to which extent) and to determine its structural and physical properties. The two end members of the solid solution, namely $MAPbBr_3$ and $DMAPbBr_3$, show a cubic 3D perovskite structure (orange color) and a 2D hexagonal structure (white color), respectively.[7] The tolerance factors of the two compounds, calculated on the basis of the following formula:

$$t = \frac{r_A + r_B}{\sqrt{2}(r_B + r_X)} \qquad (1)$$

where r_A, r_B and r_X are the ionic radii of the monovalent and bivalent cations, and of the halide, respectively, is 0.890 ($MAPbBr_3$) and 1.01 ($DMAPbBr_3$).[7,17] For values of *t* between 0.9 and 1 a cubic perovskite is expected, while for values of $t>1$ an hexagonal non-perovskite structure is predicted, which is in agreement with the room-temperature crystal structures found for the two end members of the $MA_{1-x}DMA_xPbBr_3$ system. All the intermediate compositions between $x=0$ and $x=1$, based on formula (1) and the reported ionic radii, should lead to cubic perovskite compounds (see Table 1 in the Supporting Information).

In the following, we are going to provide evidence of the existence of mixed MA/DMA lead bromide samples, also establishing the solubility limit of DMA into $MAPbBr_3$. The synthesized samples have been characterized by means of X-ray diffraction, solid-state NMR and optical spectroscopy.

Experimental Section

For the synthesis of the samples of formula $MA_{1-x}DMA_xPbBr_3$ ($0 \leq x \leq 1$), a proper amount of Pb acetate is dissolved in an excess of HBr under nitrogen atmosphere and stirring. The solution is heated to 100 °C and the corresponding amine solution (25–40% in water) is added in the required molar amounts. Usually, a precipitate is formed immediately after the amine addition. The solution is then cooled down to 46 °C at 1 °C/min, and the precipitate is immediately filtered and dried under vacuum overnight. The crystal structure of the samples was characterized by room-temperature Cu-radiation powder X-ray diffraction (XRD) on a Bruker D8 diffractometer working in the Bregg-Brentano geometry. Scans were performed in the 10–90° range, with a step size of 0.02° and a counting time of 8 s/step. Data were fitted by a Le Bail method using the FullProf suite of programs.[18]

Solid-state NMR measurements: Solid-state NMR spectra were acquired with a Bruker Avance II 400 Ultra Shield instrument, operating at 400.23 and 100.63 MHz, respectively for ^{1}H and ^{13}C nuclei. Powder samples were packed into cylindrical zirconia rotors with a 2.5 mm o.d. and a 14 μL volume. A certain amount of sample was collected from each batch and used without further preparations to fill the rotor.

^{13}C CPMAS spectra were acquired at room temperature at a spinning speed of 10 kHz, using a ramp cross-polarization pulse sequence (90° ^{1}H pulse = 2.5 μs; contact time = 2 ms) with optimized recycle delays of 16 and 32 s for pure $DMAPbBr_3$ and $MAPbBr_3$, respectively and of 240 s (for the solid solutions), and a number of scans in the range 160-1840, depending on the sample. For each spectrum, a two-pulse phase modulation (TPPM) decoupling scheme was used with a radiofrequency field of 87.7 kHz. ^{1}H MAS spectra were acquired at room temperature at a spinning speed of 32 kHz using a depth sequence, with a 90° ^{1}H pulse of 2.5 μs optimized recycle delays (>5*T_1 ^{1}H) of 16 and 32 s (for pure $DMAPbBr_3$ and $MAPbBr_3$, respectively) and of 240 s (for the solid solutions), and a number of scans of 16. The ^{1}H and

^{13}C chemical shift scales were calibrated through the ^{1}H signal of external standard adamantane at 1.87 ppm and the ^{13}C methylenic signal of external standard glycine at 43.7 ppm.

Optical properties measurements: Diffused reflectance (R) measurements were performed by using an Agilent Cary 5000 UV-Vis-NIR spectrometer. Time-resolved photoluminescence. Samples were excited by a regenerative amplifier laser (Coherent Libra) delivering 100-fs-long pulses at a repetition rate of 1 KHz. Photoluminescence was dispersed with a grating spectrometer (Princeton Instruments Acton SpectraPro 2300i equipped with a 50 gr/mm grating blazed at 600 nm), dispersed and detected by a streak camera (Hamamatsu)

Steady-state photoluminescence spectra for the bulk samples in solid state were obtained at room temperature on a Varian Cary Eclipse Fluorescence spectrophotometer with an excitation wavelength set at 550 nm.

Results and Discussion

We attempted the synthesis of samples of the $MA_{1-x}DMA_xPbBr_3$ system for x = 0, 0.05, 0.15, 0.3, 0.4, 0.5, 0.6, 0.7, 0.8, 0.9 and 1. A picture of the appearance of the samples is reported in Figure 1.

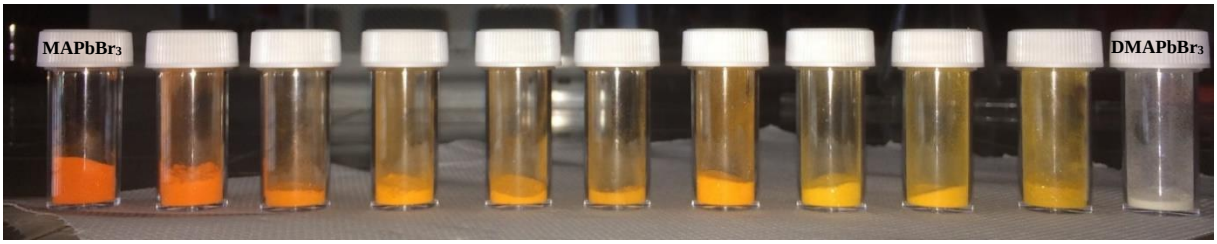

Figure 1. Appearance of the samples of the $MA_{1-x}DMA_xPbBr_3$ system for x = 0, 0.05, 0.15, 0.3, 0.4, 0.5, 0.6, 0.7, 0.8, 0.9 and 1 (from left to right).

As can be seen, $MAPbBr_3$ (first sample from the left) presents the typical orange colour, being characterized by a band-gap around 2.20 eV, while the $DMAPbBr_3$ sample (last sample on the right) is white, according to its band-gap of about 3.03 eV.[7] A progressive change of colour from x = 0 is observed, with the intermediate powders being yellow. Such trend visually suggests a progressive variation of the chemical composition of the samples prepared which has been investigated in the following. First of all, x-ray diffraction (XRD) measurements were performed on all the synthesized samples and are reported in Figure 2a.

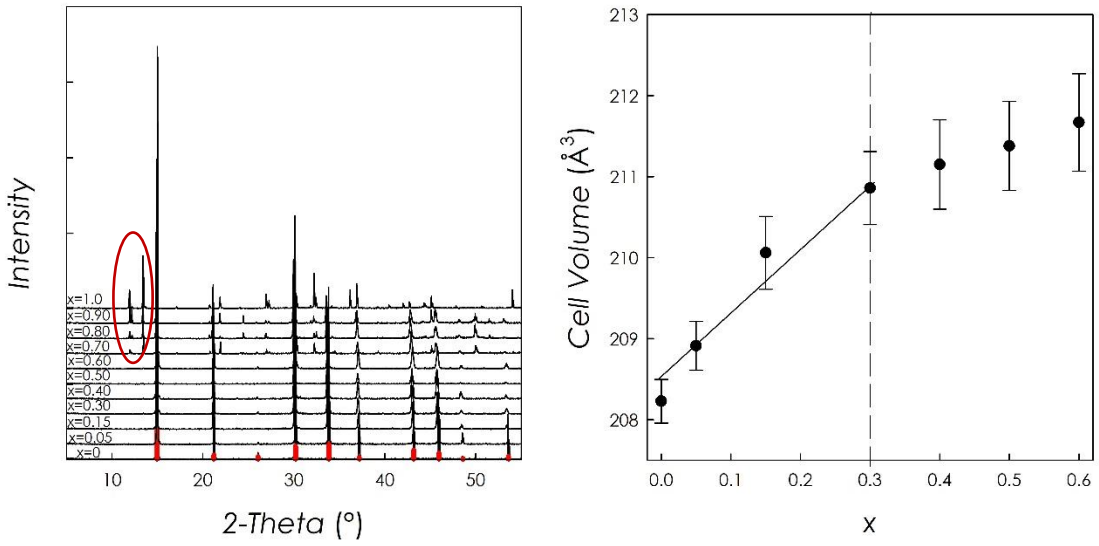

Figure 2. a) XRD patterns of the samples of the $MA_{1-x}DMA_xPbBr_3$ system for x = 0, 0.05, 0.15, 0.3, 0.4, 0.5, 0.6, 0.7, 0.8, 0.9 and 1; b) Cell volume trend vs *x*.

$MAPbBr_3$ is characterized by a cubic structure (space group: *Pm*-3*m*) while $DMAPbBr_3$ shows by an hexagonal structure (space group: $P6_3/mmc$) as previously determined from single-crystal XRD data.[7] Intermediate compositions, with the resolution provided by the present laboratory XRD data, appear to be single-phase up to about $x = 0.6$. On the other hand, for $x = 0.7$, 0.8 and 0.9, two-phase systems are clearly found (stressed by the red circle highlighting the hexagonal $DMAPbBr_3$ phase in the patterns). The single-phase compositions resulted to have the same cubic structure as $MAPbBr_3$, according to the Rietveld refinement of the patterns (vertical bars of the *Pm*-3*m* cubic structure reported at the bottom of Figure 2a). By increasing the DMA content, the peaks tend to shift to lower angles up to about ~ 0.3, together with an increase of the Full Width at Half Maximum (FWHM).

From the analysis of the XRD data, the cell volume was determined as a function of the DMA content (*x*) and is reported in Figure 2b. In the Figure, the results for the samples which appear to be single-phase from the patterns are shown. As can be appreciated from the trend of lattice volume (*V*) as a function of *x* (DMA content), a linear trend, according to Vegard's law of solid solutions, is found up to $x = 0.3$. After this composition, the cell volume variation

flattens and results to be within the standard deviation. This is strong proof that the *real* solubility of bigger DMA into the $MAPbBr_3$ structure is effective only to a DMA content around 0.3, in spite of a tolerance factor prediction of a wider solid solubility. The cell volume in the single-phase region (marked with a vertical dashed line) increases from about 208.2 $Å^3$ ($x = 0$) to about 211.2 $Å^3$ ($x = 0.3$) (lattice volume values for all the samples are reported in the SI).

To get further insight into the *real* composition of the present samples, we performed solid-state NMR, in an analogous way to our previous and pioneering approach to mixed cation systems.[19,20] Indeed, thanks to its multinuclear approach, solid-state NMR has been widely used to characterize lead halide perovskites in both bulk and thin film form.[15,21] Such technique results to be of pivotal importance in defining the effective stoichiometry of mixed organic cation systems as well as in probing the cation dynamics.[22] In the present case, it was a key tool in defining the limits of the existence of the $MA_{1-x}DMA_xPbBr_3$ solid solution by means of ^1H MAS and ^{13}C CPMAS spectra. ^1H and ^{13}C chemical shifts are listed in Table 1. The ^1H MAS spectra of $MAPbBr_3$, $DMAPbBr_3$ and of the solid solutions with $x = 0.15$, 0.3 and 0.6 are reported in Figure 3. The ^1H MAS spectrum of $MAPbBr_3$ is characterized by two resonances at 3.0 and 6.0 ppm with ratio of 1:1 for the $-CH_3$ and $-NH_3^+$ protons, respectively. The spectrum of $DMAPbBr_3$ is very similar to that of $MAPbBr_3$, with a difference in chemical shifts of 0.1 ppm for both resonances and in the signal ratio of 3:1 for the $-(CH_3)_2$ and $-NH_2^+$ protons. The composition of the solid solutions with $x = 0.15$, 0.3 and 0.6 (synthetic ratio) has been evaluated from the peak integral values (see Table 1) of the corresponding spectra. As reported in Table 1, the integral values are remarkably consistent for the compositions with $x = 0.15$. On the other hand, the sample with $x = 0.3$ and 0.6 results with only a 21.6 and 22.9% of DMA, respectively

Table 1: ^{1}H and ^{13}C chemical shifts (ppm) with integral values and experimental x value (%) for the $MA_{1-x}DMA_xPbBr_3$ system for x=0, 0.15, 0.3, 0.6 and 1. The estimated error in the experimental x value is 1.2 and 2.4% for ^{1}H and ^{13}C data, respectively.

^{1}H MAS SSNMR					
	$MAPbBr_3$ (x = 0)	**$DMAPbBr_3$ (x = 1)**	**x = 0.15**	**x = 0.3**	**x = 0.6**
Methyl δ (ppm)	3.0	3.1	3.0	3.0	3.0
Ammonium δ (ppm)	6.0	6.1	6.0	6.0	6.0
Methyl integral value	1	3	1.23	1.31	1.33
Ammonium integral value	1	1	1	1	1
Experimental x value (%)	0	100	16.3	21.6	22.9
^{13}C CPMAS SSNMR					
	$MAPbBr_3$ (x = 0)	**$DMAPbBr_3$ (x = 1)**	**x = 0.15**	**x = 0.3**	**x = 0.6**
MA δ (ppm)	29.9	-	29.9	29.9	29.9
DMA δ (ppm)	-	40.3	41.3	41.3	41.3
MA integral value	1	-	3.17	1.92	1.69
DMA integral value	-	1	1	1	1
Experimental x value (%)	0	100	13.6	20.7	22.8

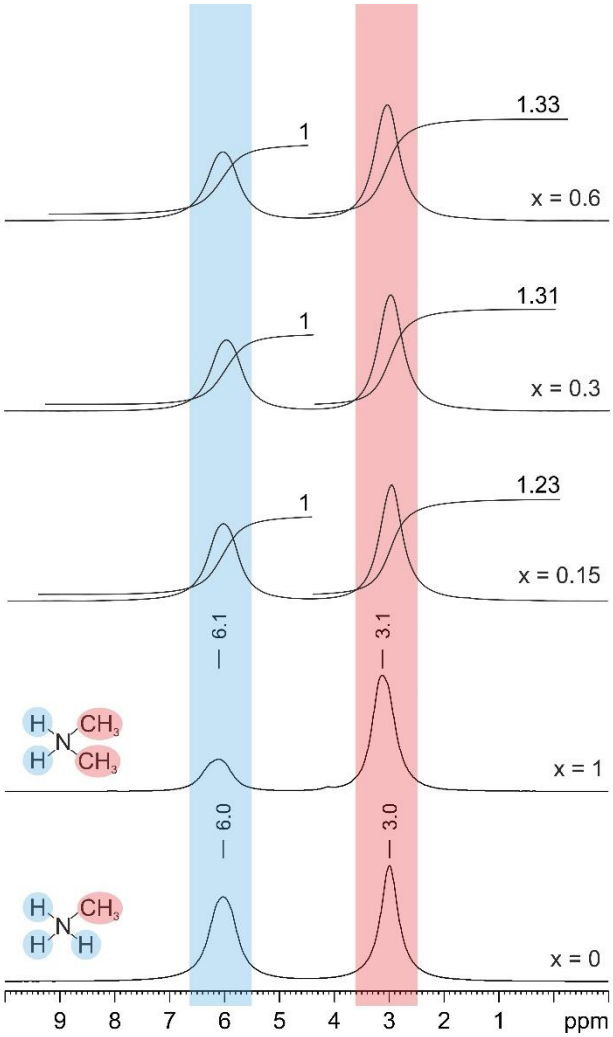

Figure 3. ^{1}H (400.23 MHz) MAS spectra of the $MA_{1-x}DMA_xPbBr_3$ system for x=0, 0.15, 0.3, 0.6 and 1, recorded at 32 kHz. Red and blue regions highlight the resonances of the methyl and ammonium protons, respectively. Integral values for the solid solutions are also reported.

A similar analysis has been performed by ^{13}C CPMAS spectra (Figure 4). In this case, $MAPbBr_3$ and $DMAPbBr_3$ are characterized by signals at very different chemical shifts: 29.9 and 40.3 ppm for MA and DMA, respectively, providing a very simple way to detect their concomitant presence. Interestingly, in the solid solutions the DMA signal slightly shifts with respect to pure $DMAPbBr_3$ probably because of the environment variation. Although the CPMAS technique is not completely quantitative, as the signal intensity depends on both T_{XH} (cross-polarization rate) and $T_{1\rho}^{H}$ (proton spin-lattice relaxation in the rotating frame), we performed a quantitative analysis also on the ^{13}C spectra. By assuming very similar cross-polarization rates and $T_{1\rho}^{H}$ for the MA and DMA cations, the semi-quantitative analysis (see Table 1) results comparable with the fully quantitative ^{1}H approach. Thus, both ^{1}H and ^{13}C solid-state NMR data show that the maximum solubility limit of DMA in $(MA/DMA)PbBr_3$ mixed cation hybrid perovskites is reached with $x \approx 0.23$.

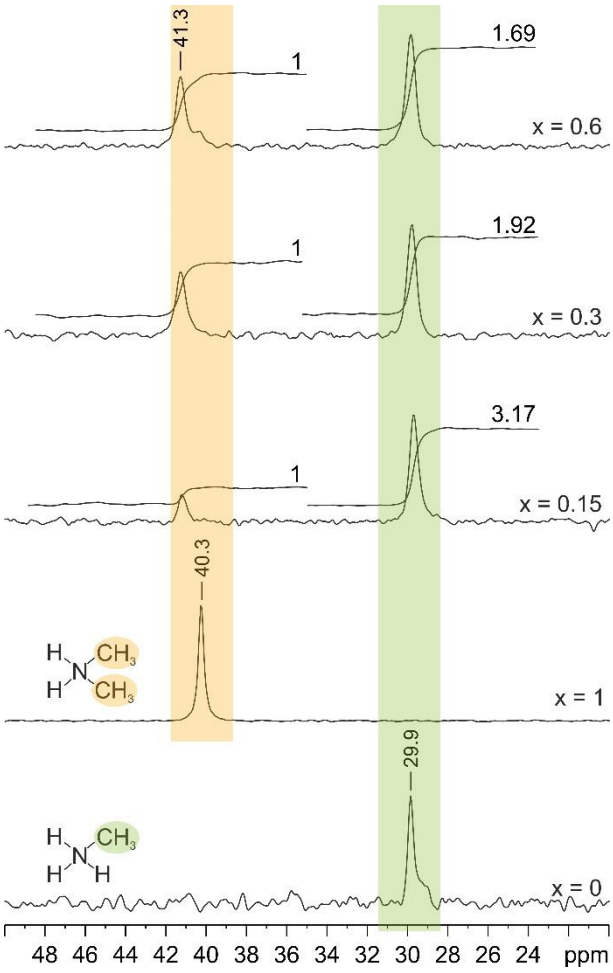

Figure 4. ^{13}C (100.63 MHz) CPMAS spectra of the $MA_{1-x}DMA_xPbBr_3$ system for x=0, 0.15, 0.3, 0.6 and 1, recorded at 10 kHz. Green and orange regions highlight the resonances of the methyl groups for $MAPbBr_3$ and $DMAPbBr_3$, respectively. Integral values for the solid solutions are also reported.

The optical properties of the single-phase samples ($0 \leq x \leq 0.3$) have been measured by means of Diffuse Reflectance spectroscopy (DRS) and photoluminescence (PL). Figure 5 shows the absorption spectra of the $MA_{1-x}DMA_xPbBr_3$ samples as a function of wavelength. A small while progressive blue-shift can be seen by increasing the amount of bigger DMA cations, which may be essentially related to the overall increase of the lattice volume, since the organic cation does not contribute to the electronic structure of the hybrid perovskites.[14] The band-gap determined from the DRS data shows an overall variation from 2.17 eV (x = 0) to 2.23 eV (x = 0.3), in agreement with the colour change of the samples (Figure 1). A similar blue shift is also

observed in the PL spectra, as shown in Fig. 5b. The PL intensity shows a multiexponential decay in all the samples, with a slightly faster recombination in the mixed cation powders (see Figure 2 of SI). A further confirm, together with the solid-state NMR data, of the solubility limit around x = 0.3, comes from the fact that all the DRS spectra above this composition are superimposable with each other up to this DMA-content value (see Figure 1 in the SI).

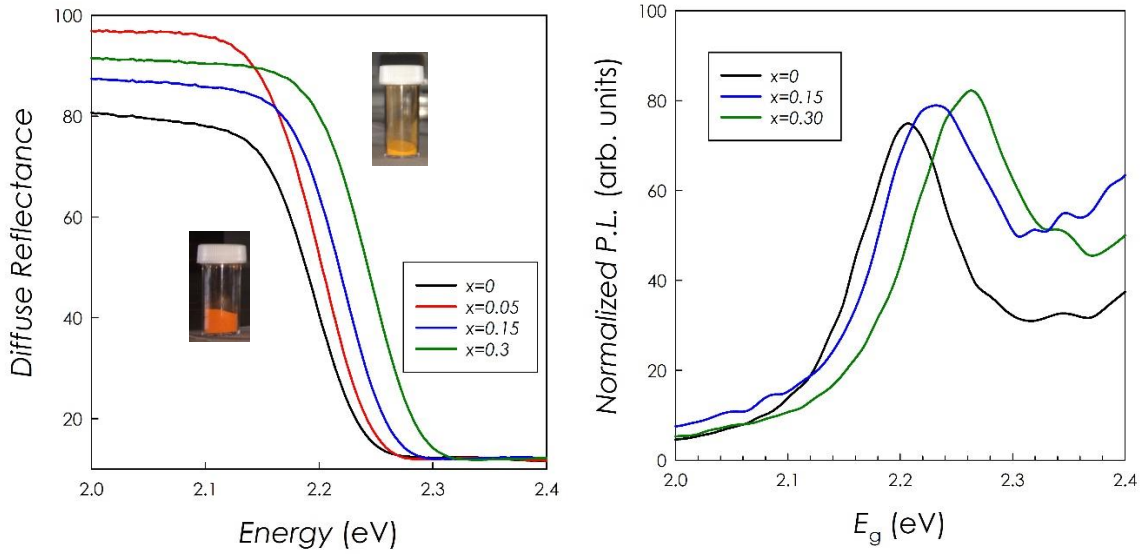

Figure 5. a) Diffuse reflectance spectra for the samples of the $MA_{1-x}DMA_xPbBr_3$ system for x = 0, 0.05, 0.15, 0.3; b) PL spectra of the $MA_{1-x}DMA_xPbBr_3$ system for x = 0, 0.15, 0.3.

The overall variation of the band-gap of about 50 meV passing from $MAPbBr_3$ to $MA_{0.70}DMA_{0.30}PbBr_3$ is in general agreement with the shift observed, for example, in the MA/FA mixed system for analogous mixed cation stoichiometries.[14] In addition, there is a linear scaling of the E_g value with the lattice volume, suggesting the predominance of structural effects on the optical properties variations observed in the PL. However, it should be noted that the agreement is in terms of absolute value of the band-gap shift but, contrary to other systems, by increasing the unit cell volume the mixed MA/DMA perovskites show a blue-shift instead of a red-shift.[23] It is not obvious to understand the origin of this peculiar behaviour which has been observed in few systems (mainly as a function of temperature) and assigned to possible effects on the electronic structure.[24] Also recent bonding analysis in metal halide perovskites

discussed the energy-gap trend in relation to the nature and magnitude of chemical bonding instead of ion-size derived approaches which demands for a detailed electronic structure analysis of the present system as a future object.[25]

It should be noted that even though the blue-shift observed up to the DMA solubility limit is not very big, that is enough to deeply change the absorption and the emission properties of the $MAPbBr_3$ lattice, including also a reduction of the carrier life-time. This means that great care should be taken when dealing with solution-based film preparation methods employing DMF as a solvent since a relatively extended solubility of DMA is found in methylammonium lead bromide which may in turn affect the optical properties of the photovoltaic active layer.

Conclusions

In the present paper the possible formation of mixed (MA/DMA)$PbBr_3$ compositions has been explored in the bulk form. The reported results indicate that the system is single-phase, with a cubic symmetry peculiar of $MAPbBr_3$, for DMA contents up to 30%. Above this threshold, DMA cannot be incorporated anymore in the lattice, as demonstrated by solid-state NMR, giving also origin to clear two-phase compositions starting from x=0.60 in the $MA_{1-x}DMA_xPbBr_3$ system. The retention of a cubic lattice for mixed MA/DMA compositions is in agreement with the trend of tolerance factor, which however cannot explain the existence of a limited solubility range on the basis of pure geometrical considerations. The optical properties show a progressive blue-shift by increasing the DMA content coupled to a slightly reduced carrier lifetime in the mixed cation compositions. Such blue-shift accompanying the incorporation of a bigger cation (DMA) differs from the usual trend found in mixed cations hybrid perovskites, indicating a possible impact on the electronic structure. In recent times there has been a strong evidence that, when employing DMF as solvent in the solution-based methods for films growth, together with concentrated HX acids, there is a tendency towards the formation of DMA cations and their possible incorporation into the hybrid perovskite lattice. This paper reports the evidence of DMA solubility in the $MAPbBr_3$ hybrid perovskite to a relevant extent, which should be taken into account when analysing the properties of films prepared as reported above.

Supporting Information

Trend of calculated tolerance factors; diffuse reflectance and time-resolved PL measurements.

Acknowledgement

The authors gratefully acknowledge the project PERSEO-"PERrovskite-based Solar cells: towards high Efficiency and lOng-term stability" (Bando PRIN 2015-Italian Ministry of University and Scientific Research (MIUR) Decreto Direttoriale 4 novembre 2015 n. 2488, project number 20155LECAJ) for funding.

References

(1) Jeon, N. J.; Noh, J. H.; Yang, W. S.; Kim, Y. C.; Ryu, S.; Seo, J.; Seok, S. II Compositional engineering of perovskite materials for high-performance solar cells *Nature* **2015**, *517*, 476.

(2) Pellet, N.; Gao, P.; Gregori, G.; Yang, T.-Y.; Nazeeruddin, M. K.; Maier, J.; Graetzel, M. Mixed-organic-cation perovskite photovoltaics for enhanced solar-light harvesting. *Angew. Chem. Int. Ed*. **2014**, *53*, 3151.

(3) Jacobsson, T. J.; Correa-Baena, J.-P.; Pazoki, M. ; Saliba, M. ; Schenk, K.; Graetzel, M.; Hagfeldt, A. Exploration of the compositional space for mixed lead halogen perovskites for high efficiency solar cells *Energy Environ. Sci*. **2016**, *9*, 1706.

(4) Yang, W. S.; Noh, J. H.; Jeon, N. J.; Kim, Y. C.; Ryu, S.; Seo, J.; Seok, S. Il High-performance photovoltaic perovskite layers fabricated through intramolecular exchange *Science* **2015**, *348*, 1234.

(5) Binek, A.; Hanusch, F. C.; Docampo, P.; Bein, T. Stabilization of the Trigonal High-Temperature Phase of Formamidinium Lead Iodide *J. Phys. Chem. Lett*. **2015**, *6*, 1249.

(6) Yang, Z.; Chueh, C.-C.; Liang, P.-W.; Crump, M.; Lin, F.; Zhu, Z.; Jen, A. K.-Y. Effects of formamidinium and bromide ion substitution in methylammonium lead triiodide toward high-performance perovskite solar cells" *Nano Energy*, **2016**, *22*, 328-337.

(7) Mancini, A.; Quadrelli, P.; Milanese, C.; Boiocchi, M.; Sironi, A.; Patrini, M.; Guizzetti, G.; Malavasi, L. Synthesis, structural and optical characterization of APbX3 (A = methylammonium, dimethylammonium, trimethylammonium; X = I,

Br, Cl) hybrid organic-inorganic materials *J. Solid State Chem*. **2016**, *240*, 55.

(8) Charles, B.; Dillon, J.; Weber, O. J.; Islam, M. S., Weller, M. T. Understanding the Stability of Mixed A-cation lead Iodide Perovskites. *J. Mater. Chem. A* **2017**, *5*, 22495.

(9) Snaith, H. J. Perovskites: The Emergence of a New Era for Low-Cost, High-Efficiency Solar Cells. *J. Phys. Chem. Lett.* **2013**, *4*, 3623– 3630.

(10) Jeon, N. J.; Noh, J. H.; Kim, Y. C.; Yang, W. S.; Ryu, S.; Seok, S. I. Solvent Engineering for High-Performance Inorganic–Organic Hybrid Perovskite Solar Cells. *Nat. Mater.*, *13*, 897– 903.

(11) Zhou, Y.; Zhou, Z.; Chen, M.; Zong, Y.; Huang, J.; Pang, S.; Padture, N. P. Doping and alloying for improved perovskite solar cells. *J. Mater. Chem. A* **2016**, *4*, 17623– 17635.

(12) Saliba, M.; Matsui, T.; Seo, J.-Y.; Domanski, K.; Correa-Baena, J.-P.; Nazeeruddin, M. K.; Zakeeruddin, S. M.; Tress, W.; Abate, A.; Hagfeldt, A. Cesium-Containing Triple Cation Perovskite Solar Cells: Improved Stability, Reproducibility and High Efficiency. *Energy Environ. Sci.* **2016**, *9*, 1989– 1997.

(13) Daub, M.; Hillebrecht, H. On the Demystification of "$HPbI_3$" and the Peculiarities of the Non-innocent Solvents H_2O and DMF. *Z. Anorg. Allg. Chem*. **2018**, doi.org/10.1002/zaac.201800267.

(14) Franssen, W. M. J.; Bruijnaers, B. J.; Portengen, V. H. L., Kentgens, A. P. M. Dimethylammonium Incorporation in Lead Acetate Based $MAPbI_3$ Perovskite Solar Cells. *ChemPhysChem* 2018, DOI: 10.1002/cphc.201800732.

(15) Ke, W.; Spanopulos, I.; Stoumpos, C. C.; Kanatzidism M. G. Myths and Reality of $HPbI_3$ in Halide Perovskite Solar Cells. *Nature Comm.* **2018**, *9*, 4785.

(16) Kieslich, G.; Sun, S.; Cheetham, A. K.; An extended Tolerance Factor approach for organic–inorganic perovskites *Chem. Sci*. **2015**, *6*, 3430.

(17) Shannon, R. D. Revised effective ionic radii and systematic studies of interatomic distances in halides and chalcogenides. *Acta Cryst*. **1976**, *32*, 751–767.

(18) Rodriguez-Carvajal, J. Recent advances in magnetic structure determination by neutron powder diffraction *Phys. B* **1993**, *192*, 55.

(19) Pisanu, A.; Ferrara, C.; Quadrelli, P.; Guizzetti, G.; Patrini, M.; Milanese, C.; Tealdi, C.; Malavasi, L. The $FA_{1-x}MA_xPbI_3$ System: Correlations among Stoichiometry Control, Crystal Structure, Optical Properties, and Phase Stability *J. Phys. Chem. C* **2017**, *121* (16) 8746– 8751.

(20) Ferrara, C.; Patrini, M.; Pisanu, A.; Quadrelli, P.; Milanese, C.; Tealdi, C.; Malavasi, L. Wide Band-Gap Tuning in Sn-Based Hybrid Perovskites through Cation Replacement: the $FA_{1-x}MA_xSnBr_3$ Mixed System *J. Mater. Chem. A* **2017**, *5*, 9391–9395.

(21) Roiland, C.; Trippé-Allard, G.; Jemli, K.; Alonso, B.; Ameline, J.-C.; Gautier, R.; Bataille, T.; Le Pollès, L.; Deleporte, E.; Even, J.; Katan, C. Multinuclear NMR as a tool for studying local order and dynamics in $CH_3NH_3PbX_3$ (X = Cl, Br, I) hybrid perovskites. *PCCP* **2018**, *18*, 27133-27142.

(22) Kubicki, D. J.; Prochowicz, D.; Hofstetter, A.; Péchy, P.; Zakeeruddin, S.M.; Graetzel, M.; Emsley, L. Cation Dynamics in Mixed-Cation $(MA)_x(FA)_{1-x}PbI_3$ Hybrid Perovskites from Solid-State NMR. *J. Am. Chem. Soc.* **2017**, *139*, 10055-10061.

(23) Brennan, M. C.; Draguta, S.; Kamat, P. V.; Kuno, M Light-Induced Anion Phase Segregation in Mixed Halide Perovskites. *ACS Energy Lett.* **2018**, *3*, 204-213.

(24) Dar, M. I.; Jacopin, G.; Meloni, S.; Mattoni, A.; Arora, N.; Boziki, A.; Zakeeruddin, S. M.; Rothlisberger, U.; Graetzel, M. Origin of Unusual Bandgap Shift and Dual Emission in Organic-Inorganic Lead Halide Perovskites. *Science Adv.* **2016**, *2*, e1601156.

(25) Goesten, M. G.; Hoffmann, R. Mirrors of Bonding in Metal Halide Perovskites. *J. Am. Chem. Soc.* **2018**, *140*, 12996-13010.

TOC GRAPHICS

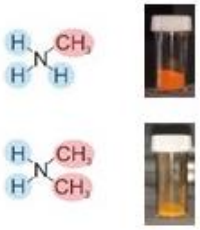

The possible incorporation of dimethylammonium (DMA) cation into the $MAPbBr_3$ hybrid perovskite has been studied for the first time. It has been found that DMA can be present up to 30% forming a mixed MA/DMA perovskite with a cubic structure. A progressive blue-shift of the band-gap is observed along with the DMA incorporation.